J. Fluid Mech. (1995), *vol.* 305, *pp.* 219–238

Thermo-viscous fingering of flow in a thin gap: a model of magma flow in dikes and fissures

By KARL R. HELFRICH

Woods Hole Oceanographic Institution, Woods Hole, MA 02543, USA

(Received 24 January 1995 and in revised form 2 August 1995)

Flow of a fluid with a strongly temperature-dependent viscosity in a finite-length slot is analysed as a model of magma flow in dikes. The slot walls are held at a fixed temperature, thus cooling and increasing the viscosity of the fluid as it moves along the gap. Poiseuille flow and temperature advection, averaged across the slot, are used to study the stability of this basic one-dimensional flow to lateral perturbations. A linear stability analysis shows that for sufficiently strong cooling and viscosity increase with decreasing temperature, the flow is unstable to a fingering instability. Warm fluid is focused into relatively fast flowing zones and suffers only modest cooling, while cold, slow flowing regions experience more cooling and an increase in viscosity, which acts to locally clog the slot. The necessary condition for instability is the presence of multiple solutions for velocity (fast, intermediate and slow branches) in the basic one-dimensional flow. The intermediate branch, where the thermal adjustment lengthscale is comparable to the slot length, is unstable and the analysis indicates that the instability continues onto the slow branch. The parametric regions of instability and the growth rates are dependent on the choice of boundary conditions at the slot entrance (i.e. the magma source): either uniform flux, or uniform pressure. The latter case is the more geophysically realistic and has the larger unstable region and growth rates. Numerical solutions of the nonlinear equations show that at finite-amplitude the hot, low-viscosity, fast-flowing fingers continue to speed up, while the slow, cold regions continue to cool and slow down. At the slot exit fluid issues from the gap in isolated hot, low-viscosity spouts separated by zones of cold, nearly still fluid. Application of the model to geophysical settings indicates that the instability is expected for realistic parameter values. The model may help explain the observed focusing of fissure eruptions.

1. Introduction

There are many geophysical situations in which a viscous fluid is cooled as it flows. If the viscosity of the fluid increases as the temperature decreases, the resistance to the flow will increase. The extreme case is when the material freezes and completely stops flowing. However, if the flux must be maintained due to a continuous source, then this type of thermo-viscous rheology can lead to complex behaviour. For example, in the spreading of viscous gravity currents surface cooling can lead to a variety of morphological structures including pillow lava features, rifts and folds (Fink & Griffiths 1990) and sharp, shock-like, fronts (Bercovici 1994). Another example is the observed focusing of flow in magmatic fissure eruptions (Richter *et al.* 1970; Delany & Pollard 1982). These eruptions often begin as a uniform flux from a long

linear fissure. Over time the flow becomes focused into isolated spouts separated by segments of the fissure which have closed.

The dynamics of this flow focusing and the related issue of freezing and melt-back of dike walls have been the subject of a several of previous studies. Fujii & Uyeda (1974) showed that in a one-dimensional problem (cross-gap variations only) the combination of temperature-dependent viscosity and frictional heating results in a thermal instability leading to infinite flux when a critical condition is exceeded. However, their analysis did not allow for variability in the lateral direction, or for changes in the direction of the flow, and so could not produce a condition for the development of spatial fingering. Bruce & Huppert (1989, 1990) and Turcotte (1990) improved upon this type of analysis by developing models of the thermodynamics of freezing and melt-back of the gap walls in a slot of finite length. For a given rheology and physical setting (driving pressure gradient, surrounding wall rock temperature, initial temperature at the source, slot length, etc.) these models predict that a slot narrower than a critical width will freeze shut and the flow will decrease. For larger initial gaps the walls will melt back and allow an increased flux. Bruce & Huppert (1989, 1990) used their model to suggest that the lateral focusing of fissure eruptions arises from the initial variability in the fissure width (in the lateral direction) with some areas giving rise to freezing and others melt-back.

Whitehead & Helfrich (1991, hereafter referred to as WH) investigated a different model in which fluid rheology and thermodynamics combine internally to produce temporal and spatial structure. Cooling of the fluid as it flows through a finite-length cylindrical tube results in increased viscosity and therefore resistance to the flow. This causes an increase in the driving pressure gradient (the fluid source is a continuously fed elastic chamber) which eventually becomes large enough to rapidly force the cold fluid out of the tube. The driving pressure then decreases and consequently so does the flux. The fluid in the tube then cools and the pattern repeats. The result is a limit cycle: periods of rapid hot flow and periods of slow cold flow. A requirement for the instability and limit cycle was the occurrence of multiple solutions to the steady-state relation between pressure drop along the tube length and the mass flux (discussed in more detail below). Laboratory experiments supported the model results.

WH's extension of the model to two dimensions (a cooled planar slot), but with all the lateral flow occurring in the underlying elastic chamber, gave rise to a spatial fingering instability. Hot, low-viscosity, fast-flowing fluid zones alternated with cold, high-viscosity, slow-flowing zones. This two-dimensional fingering is related to the familiar Saffman–Taylor instability, but where the flow internally determines the viscosity structure. Again the necessary condition for instability is multiple solutions for the basic-state pressure–flow relation. Their linear model predicted that the growth rate was the same for almost all wavenumbers. No specific wavenumber was expected to dominate based upon a largest linear growth rate. Some preliminary laboratory experiments showed that low wavenumbers were preferred, and thus it appears that the model is inadequate. Further, the WH model retained inertia terms in the momentum equations and quasi-steady heat advection. For the viscously dominated, high Prandtl number flows under consideration time-dependence in the heat equation is important, while inertia in the momentum equation is not.

In this paper a theory of the type discussed by WH is presented in which lateral flow in the slot is allowed, but in which the details of the fluid source region (i.e. the magma chamber) are ignored other than as a specification of the slot inflow boundary condition. The structure across the thin gap is treated as in the Hele-Shaw approximation by averaging the viscosity, velocity and temperature across the gap.

Time-dependence is retained only in the temperature equation and heat loss to the surrounding solid walls is modelled using a linear heat transfer law. The present model is less realistic that the model of Bruce & Huppert (1989, 1991) in that no account is taken of the cross-gap structure of the flow, viscosity and temperature. But the present model does add the lateral dimension to the problem. Freezing and melt-back of the gap walls are not considered, rather the focus here is on a fluid with strongly temperature-dependent viscosity.

In §2 the governing equations and boundary conditions are given. The basic-state flow is discussed in §3. It is shown that for a large enough cold to hot viscosity ratio there exist multiple solutions for the basic-state fluid velocity: slow, intermediate and fast branches. In §4 the linear stability of this basic state is studied. It is shown that for either of the two choices of source boundary conditions, fixed uniform flux or uniform pressure, the flow may be subject to a fingering instability in which hot fluid is focused into fast-flowing channels separated by cold, slow-flowing viscous regions. The constant-pressure case generally has the higher growth rates and larger parametric region of instability. Both cases predict a maximum growth rate and a short-wave cutoff of the instability, while only the uniform flux case always has a long-wave cutoff.

In §5 the nonlinear equations are solved numerically to study the finite amplitude evolution of the instability. The calculations show that at finite amplitude the flow focusing continues, leading to faster flow in the hot channels and zones of slowing and cooling flow. This pattern is apparently stable and is not subject to secondary instabilities. For general initial conditions low wavenumbers are preferred at finite amplitude. In §6 the results are summarized and application of the model to the motivating geophysical problem is discussed.

2. The model

The physical situation is shown in figure 1. Hot fluid with temperature T_H and viscosity μ_H is forced into a thin slot of width $d << L$, where L is the length of the slot in the z-direction. The slot is taken to be infinite in the lateral dimension x. The flow is assumed to be laminar and dominated by friction and pressure and the Prandtl number to be large. Under these assumptions the velocity $\boldsymbol{u} = (u, w)$, where u is the velocity in the x-direction and w is the z-direction velocity, and temperature T, averaged across the gap are governed by

$$\frac{12\mu}{d^2}\,\boldsymbol{u} = -\nabla p + g\boldsymbol{k}\rho_H\alpha'\,(T - T_H), \tag{1}$$

$$\nabla \cdot \boldsymbol{u} = 0, \tag{2}$$

and

$$\frac{\partial T}{\partial t} + \boldsymbol{u}\cdot\nabla T = \kappa\nabla^2 T - \delta'(T - T_W). \tag{3}$$

Here p is the departure of the pressure from hot hydrostatic ($\partial p/\partial z = -\rho_H g$), $\mu(T)$ is the fluid viscosity and $\nabla = (\partial/\partial x,\ \partial/\partial z)$. Here t is time, g is the gravitational acceleration, $\boldsymbol{k}$ is the unit vector in the z-direction, ρ_H is the density at the entrance temperature T_H. The momentum equation (1) includes the effect of fluid buoyancy using a linear equation of state with the thermal expansion coefficient α'.

The thermal diffusivity of the fluid κ is assumed constant. Heat loss to the

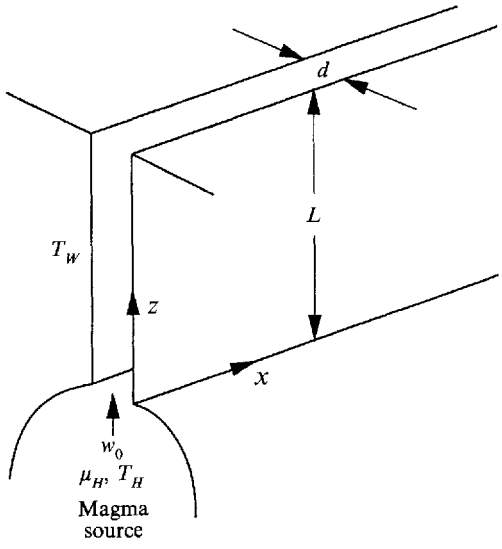

FIGURE 1. Definition sketch.

surrounding solid walls is approximated by the last term in (3), where the heat transfer coefficient

$$\delta' \approx \frac{\pi^2 \kappa}{d^2} . \tag{4}$$

This assumes that the temperature field is dominated by the first sine mode in the cross-gap direction. The temperature of the surrounding solid rock is T_W. More rigorous treatments of the thermodynamics are certainly possible (for example see Bruce & Huppert 1989, 1990), but for this study T_W is taken as a constant. Heating of the wall rock is ignored and so the analysis should be considered valid only for times less than a thermal diffusion time d^2/κ_W, where κ_W is the diffusivity of the wall rock. For typical values of $d = 1$ m and $\kappa_W = 10^{-6}$ m^2 s^{-1}, this corresponds to $t < 10$ days. For comparable and longer times the heat loss to the surrounding wall rock effectively insulates the magma and δ' should decrease as $t^{-1/2}$.

The viscosity is taken to be a strongly increasing function for decreasing temperature as is appropriate for magma in the neighbourhood of the solidus temperature. For simplicity the formula

$$\mu = \mu_H e^{\gamma'(T_H - T)} , \tag{5}$$

where γ' is a constant, is used. This relation was used by Fujii & Uyeda (1974). However, it is only an approximation for real magmas which can have complex rheologies in the temperature range near their solidus temperature (Shaw 1969; Ryan & Blevins 1987).

The use of the Hele-Shaw (i.e. averaged) model for this temperature-dependent viscosity problem is also a significant approximation. First it assumes that the flow is laminar. This is reasonable for basaltic magma flow in narrow fractures ($d < 1$–2 m) where the driving pressure is provided principally by the buoyancy difference between the magma and the surrounding rock (Turcotte 1990). The important role of viscosity in these flows has also been demonstrated in analysis of fluid mechanical models of crack propagation (Lister & Kerr 1991; Lister 1994*a*,*b*). A Reynolds number based on the gap width is typically $\leqslant O(10)$. This combined with the assumptions of narrow gap, $d/L << 1$, and high Prandtl number, $\mu/\rho\kappa >> 1$, leads to the balance between

friction and pressure represented by (1) and the retention of time-dependence in the temperature equation (3).

More significantly, cooling at the walls will give rise to a cross-gap viscosity profile and subsequent modification of the velocity profile from the parabolic shape of the constant-viscosity Poiseuille problem. The temperature field will also be affected. This will in turn modify the integrated mass and heat fluxes through the gap (Ockendon & Ockendon 1977). Bercovici (1994) has shown that even after accounting for this cross-gap viscosity and velocity structure, the average velocity can still be modelled by the momentum equation (1) with viscosity function replaced by a modified form. In general, this effect can be shown to require a lower value of γ' in the averaged model than the actual γ' of the fluid. This is because in the non-averaged problem cooling and viscosity increase at the channel walls where the velocity is lowest. This reduces the effective channel width, and therefore increases the average resistance to the flow (expressed as $12\mu/d^2$ in (1)) while also promoting cooling of the core of the flow. The combination of wall cooling and channel constriction can be parameterized as an increase in the average viscosity, but with a weaker dependence on temperature than the viscosity of the actual fluid, hence a smaller γ'.

The cross-gap structure is certainly an important aspect of the complete problem, but to illustrate the basic thermo-viscous instability and assess the relevance of the phenomenon for the geophysical situation, an averaged model is used. Certainly the good qualitative agreement between experiments and theory obtain by WH in the one-dimensional problem suggests that an averaged model captures the essential physics.

During the preparation of this paper the author became aware of recent work by Wylie & Lister (1995) who have studied the same problem without averaging in the cross-gap direction. Their work shows that the averaged model does lead to qualitatively correct results, though quantitative differences will be present. This is addressed in §6. One feature of this study not fully considered in theirs is the nonlinear development of the flow.

The governing equations (1)–(3) and the viscosity (5) are normalized with the following scales:

$$(x, z) \rightarrow L,$$

$$t \rightarrow L/U,$$

$$(u, w) \rightarrow U = \frac{Pd^2}{12L\mu_H},$$

$$T \rightarrow (T_H - T_W),$$

$$\mu \rightarrow \mu_H.$$

The velocity scale U follows from the Poiseuille relation for fluid with viscosity μ_H and a driving pressure gradient of P/L.

The streamfunction ψ, where

$$(u, w) = (-\psi_z,\ \psi_x), \tag{6}$$

is defined. Eliminating p from (1) and using (6) gives the vorticity equation

$$\nabla^2\psi = -\frac{\mathrm{d}\ln\mu}{\mathrm{d}\theta}\,\nabla\psi\cdot\nabla\theta + \frac{\alpha}{\mu}\,\frac{\partial\theta}{\partial x}. \tag{7}$$

The temperature equation (3) and the viscosity (5) become, respectively,

$$\frac{\partial \theta}{\partial t} + J(\psi, \theta) = -\delta\theta \tag{8}$$

and

$$\mu = \mathrm{e}^{\gamma(1-\theta)} . \tag{9}$$

The Jacobian $J(a, b) = a_x b_z - a_z b_x$. The scaled temperature θ is

$$\theta = \frac{T - T_W}{T_H - T_W} . \tag{10}$$

The non-dimensional coefficients δ, γ and α are

$$\delta = \frac{\delta' L}{U} = \frac{12\pi^2 \kappa \mu_H L^2}{P d^4}, \quad \gamma = \gamma'(T_H - T_W) , \quad \alpha = \frac{g\rho_H \alpha' (T_H - T_W) L}{P} . \tag{11}$$

The ratio of cold to hot viscosities is e^{γ}.

In (8) heat diffusion has been neglected, except for the component from the fluid to the wall (i.e. δ). This is justified since the Péclet number $UL/\kappa = O(10^9)$ for the typical values $U = 1$ m s^{-1}, $L = 10^3$ m and $\kappa = 10^{-6}$ m^2 s^{-1}. The temperature field is dominated by advection and heat loss through the walls.

The dynamic boundary condition at the slot exit is

$$u = -\psi_z = 0 \qquad \text{at } z = 1. \tag{12}$$

This follows from (1) and the assumption that pressure is uniform at the exit. Temperature is simply advected out of the slot. In specifying these outlet conditions it is assumed that once fluid leaves the gap it does not re-enter the gap or affect the following fluid parcels. Effectively, fluid is removed immediately from the slot exit region. At the entrance to the slot ($z = 0$) fluid temperature is T_H and so

$$\theta = 1 \qquad \text{at } z = 0. \tag{13}$$

The dynamic condition at $z = 0$ can take either of two forms. In the first case (hereafter called Case I) flow into the slot is uniform in x and constant in time, but the pressure is not constant along the slot entrance. In the second case (Case II) the pressure at $z = 0$ is constant (i.e. $\partial p/\partial x = 0$). This second condition allows the flow into the slot to vary with x, but the total integrated flux into the slot is maintained constant (the same as in Case I). Coupling of the slot flow to an underlying elastic source chamber is left for a later study, but from the work of WH this could be expected to give rise to interesting time-dependent behaviour. Further specification of the conditions is deferred until the §4 (equations (20) and (21)), after the basic-state flow has been introduced.

3. Basic flow

Ignoring variations and flow in the lateral direction a steady basic state with constant z-velocity w_0 is

$$\Psi = w_0 x , \quad \Theta = \mathrm{e}^{-\delta z/w_0} , \quad \mathscr{M} = \mathrm{e}^{\gamma(1-\Theta)} . \tag{14a–c}$$

Here Ψ, Θ and $\mathscr{M}$ are the basic-state streamfunction, temperature and viscosity, respectively. From (1) and (14) the pressure difference between $z = 0$ and 1, Δp, is

$$\Delta p = 1 = w_0 \int_0^1 \mathscr{M}(z)\mathrm{d}z - \frac{\alpha w_0}{\delta} (1 - \mathrm{e}^{-\delta/w_0}) + \alpha. \tag{15}$$

Note that Δp has the opposite sign from the pressure gradient.

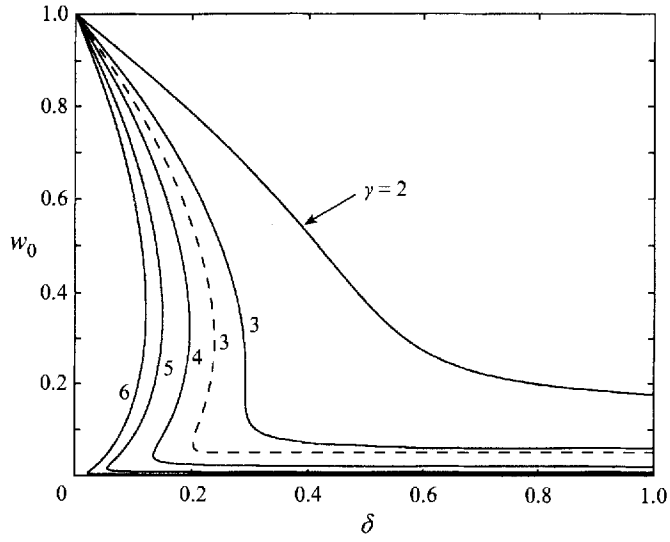

FIGURE 2. Basic one-dimensional flow velocity w_0 as a function of δ for several values of the viscosity parameter γ. The solid curves are for $\alpha = 0$. Multiple solutions for w_0 occur over a finite range of δ for $\gamma > \gamma_c = 3.03$ when $\alpha = 0$. The dashed curve is for $\gamma = 3$ and $\alpha = 0.5$.

In (15) the pressure difference Δp is normalized to 1 using the driving pressure scale P. This then gives a relationship between the basic-state velocity w_0, or flux per unit length $w_0 d$, and the external parameters δ, γ and α. The relation (15) could have been scaled so that $w_0 = 1$, in which case (15) gives a relation between Δp and the external parameters. However, in what follows we choose the first alternative since it is consistent with the geological setting of the problem where the driving pressure is the more likely independent parameter.

The behaviour of the basic flow can be explored by examining the limits of fast and slow flow. When the flow is slow, or δ is very large, such that $\delta/w_0 >> 1$, from (14*b*, *c*) $\Theta \sim 0$ and $\mathcal{M} \sim \mathrm{e}^{\gamma}$, and from (15) $w_0 \sim (1-\alpha)\mathrm{e}^{-\gamma}$. Fluid entering the channel is immediately cooled to the wall temperature and consequently the viscosity is very large and the flow is very slow. In the fast, or small-δ, limit $\delta/w_0 << 1$, $\Theta \sim 1$, $\mathcal{M} \sim 1$ and $w_0 \sim 1$. In this case the thermal adjustment scale w_0/δ is much greater than the slot length. The fluid experiences no cooling as it moves through the slot. The solutions in the intermediate regime $\delta/w_0 = O(1)$, where the thermal adjustment scale is comparable to the slot length, is more complicated and is shown in the figure 2 where w_0 is plotted as a function of δ for several values of γ with $\alpha = 0$. For small γ the relation is single valued; however, as γ is increased the relation bifurcates to give three solutions for w_0 over a range of δ for a fixed γ. For $\alpha = 0$ multiple solutions occur for all γ greater than the critical value $\gamma_c = 3.03$, or a cold to hot viscosity ratio of 20.7. Within the range of δ where three solutions exist, two of the solution branches correspond to the fast and slow solutions discussed above, and the third is an intermediate velocity solution. For δ outside this range only one solution exists.

Figure 3 shows the region of δ, γ parameter space where multiple solutions exist for $\alpha = 0$. As γ increases the range of δ for multiple solutions increases, but the trend is towards smaller δ. Larger viscosity contrasts require lower heat transfer coefficients to give multiple solutions.

Consideration of buoyancy effects with $\alpha \leqslant O(1)$ does not change the qualitative

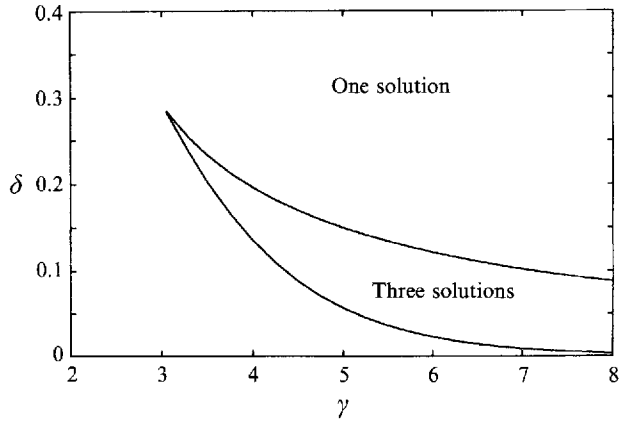

FIGURE 3. The region of δ, γ space in which multiple solutions are found for $\alpha = 0$.

behaviour, but does result in multiple solutions for lower γ when $\alpha > 0$. This is illustrated in figure 2 by the dashed line which is for $\gamma = 3$ and $\alpha = 0.5$. Multiple solutions now occur for $0.203 < \delta < 0.239$. If $\alpha < 0$ (i.e. downhill flow) the onset of multiple solutions is delayed until larger γ.

4. Linear stability

When δ, γ and α are such that multiple solutions exist and Δp, from (15), is plotted as a function of w_0, the fast and slow solution branches are seen to have $\mathrm{d}\Delta p/\mathrm{d}w_0 > 0$. On the intermediate solution branch $\mathrm{d}\Delta p/\mathrm{d}w_0 < 0$. An example is shown in figure 4 for $\gamma = 5$, $\delta = 0.1$ and $\alpha = 0$. The three solutions which occur with the scaling $\Delta p = 1$ are indicated by the circles. WH showed that a necessary condition for instability in either their one- or two-dimensional model was that $\mathrm{d}\Delta p/\mathrm{d}w_0 < 0$ over some range of w_0. It is very likely that the intermediate solution here is unstable. However, the situation here is complicated by the inclusion of lateral flow in the slot and the other model improvements. Thus linear stability of the basic state (14) to lateral perturbations is investigated.

Defining the perturbations ϕ and θ' from the basic state Ψ and Θ:

$$\psi = \Psi + \phi(x,z,t); \qquad \theta = \Theta + \theta'(x,z,t) \tag{16}$$

the vorticity (7) and temperature (8) equations become, respectively,

$$\nabla^2\phi = \left[\frac{\alpha}{\mu} + \gamma(w_0 + \phi_x)\right]\theta'_x + \gamma(\Theta_z + \theta'_z)\phi_z \tag{17a}$$

and

$$\theta'_t + w_0\,\theta'_z + \phi_x\,\Theta_z + J(\phi,\theta') = -\delta\theta', \tag{17b}$$

with μ given by (9). The boundary condition on θ' at $z = 0$ is (from (13))

$$\theta' = 0 \qquad \text{at } z = 0. \tag{18}$$

At $z = 1$ the uniform pressure condition (12) gives

$$\phi_z = 0 \qquad \text{at } z = 1. \tag{19}$$

The boundary condition of uniform vertical velocity w_0 at $z = 0$ (Case I) gives

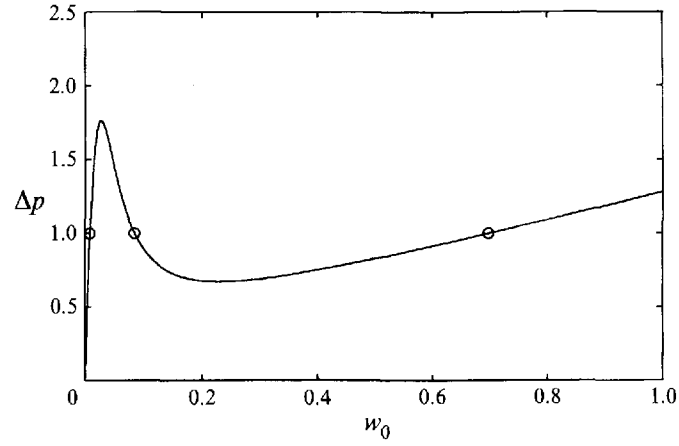

FIGURE 4. The basic-state pressure drop Δp as a function of w_0 for an example with $\gamma = 5$, $\delta = 0.1$ and $\alpha = 0$. The three solutions for w_0 at $\Delta p = 1$ are indicated by the circles. At the intermediate solution $\mathrm{d}\Delta p/\mathrm{d}w_0 < 0$, and $\mathrm{d}\Delta p/\mathrm{d}w_0 > 0$ at the fast and slow solutions.

(from (14) and (16))

$$\phi_x = 0 \qquad \text{at } z = 0, \tag{20}$$

and Case II, uniform pressure in x, gives (from (1), (14) and (16))

$$\phi_z = 0 \qquad \text{at } z = 0. \tag{21}$$

The linear stability analysis assumes solutions of the form

$$\begin{pmatrix} \phi \\ \theta' \end{pmatrix} = \begin{pmatrix} f(z)\sin kx \\ h(z)\cos kx \end{pmatrix} \mathrm{e}^{\sigma t}. \tag{22}$$

From (17*a,b*) and the boundary conditions (18), (19) and (20), or (21), the eigenvalue problem for the growth rate σ and structure functions $g(z)$ and $h(z)$ is

$$\frac{\mathrm{d}^2 f}{\mathrm{d}z^2} - \gamma \frac{\mathrm{d}\Theta}{\mathrm{d}z}\frac{\mathrm{d}f}{\mathrm{d}z} - k^2 f + k\left(\gamma w_0 + \frac{\alpha}{\mathscr{M}}\right) h = 0, \tag{23a}$$

$$w_0 \frac{\mathrm{d}h}{\mathrm{d}z} + (\sigma + \delta)h + k\frac{\mathrm{d}\Theta}{\mathrm{d}z} f = 0 \tag{23b}$$

with

$$h(0) = 0, \quad \frac{\mathrm{d}f(1)}{\mathrm{d}z} = 0 \tag{23c,d}$$

and

$$f(0) = 0 \quad \text{(Case I)} \qquad \text{or} \qquad \frac{df(0)}{dz} = 0 \quad \text{(Case II)}. \tag{23d}$$

Here k is the wavenumber in the x-direction. The phase dependence of (22) arises from the assumption that σ, g and h are real. Oscillatory solutions may exist, but because of the dissipative nature of the flow and the steady forcing these would be rapidly damped or advected from the domain. This assumption is supported by the nonlinear calculations discussed in the next section. The eigenvalue problem (23), with Θ and $\mathscr{M}$ from (14*b, c*), is solved numerically using the Runge–Kutta method with shooting.

In figure 5 contours of growth rate σ are shown in the (k, w_0)-plane for $\alpha = 0$ and $\gamma = 5$. This is well into the supercritical γ-regime but, as shown below, the behaviour

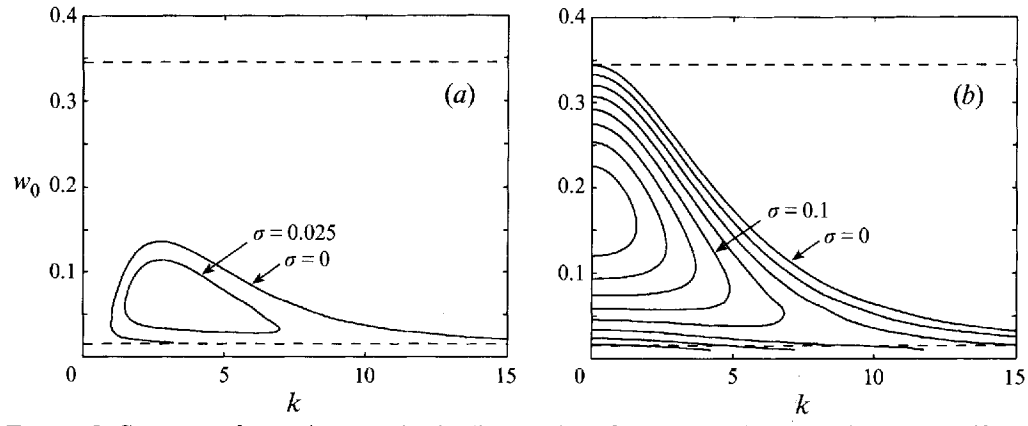

FIGURE 5. Contours of growth rate σ in the (k, w_0)-plane for $\gamma = 5$ and $\alpha = 0$. (*a*) Case I, uniform source flux boundary condition (20). (*b*) Case II, uniform source pressure boundary condition (21). The σ contour interval is 0.025. Dotted lines bound the multiple solution regime.

here is typical of all γ. The results are shown using w_0 rather than δ, since w_0 implies a unique value of δ, but not vice versa. Also indicated on the figures by the dashed lines are the values of w_0 which bound the multiple solution regime. Values of w_0 between the lines are solutions which lie on the intermediate branch of (15), those above and below are on the fast and slow branches, respectively. Only positive values of σ indicating instability are plotted. Figure 5(*a*) shows the results using the Case I, uniform source flux, boundary condition. The results from Case II, uniform source pressure, are given in figure 5(*b*).

Case I is unstable only for $w_0 < 0.136$ which is well below the maximum of the range of intermediate solutions $w_0 = [0.015, 0.345]$ (for $\delta = [0.0565, 0.149]$). The instability has both long- and short-wave cutoffs. When w_0 is small, numerical solution of the eigenvalue problem becomes difficult, but the results indicate that the slow solution branch (below the lower dashed line) may also be unstable. This behaviour is shown more clearly in figure 5(*b*) and discussed below. The maximum growth rate occurs for $k \approx 2.9$ and $w_0 \approx 0.07$. As w_0 decreases the most unstable wavenumber increases. The wavelength of the most unstable wave scales with the thermal adjustment length w_0/δ.

In contrast, Case II (figure 5*b*) shows greater overall growth rates, no long-wave cutoff for solutions on the intermediate branch and a larger parametric region of instability. The instability is present for all w_0 corresponding to the intermediate solution as $k \to 0$. The fast branch, $w_0 > 0.345$, is entirely stable. The calculations also show that just onto the slow branch of solutions ($w_0 < 0.015$) the instability persists with the unstable range in k moving to higher wavenumbers as w_0 decreases. Here the wavelength of the most unstable wave scales with w_0/δ. However, further exploration of the instability in this range proved difficult with the present numerical techniques.

Increasing or decreasing γ does not change the qualitative behaviour of the instability. Figure 6 shows the growth rates for both boundary condition choices for $\gamma = 6$ and $\alpha = 0$. The results are quite similar to those in figure 5(*a,b*). Values of γ up to 9 have been investigated and there are no qualitative changes.

Figure 7 shows the results for Case II (uniform pressure) for $\gamma = 3.25$ and $\alpha = 0$. This is just above the critical value, $\gamma_c = 3.03$, for multiple solutions. At these parameter values Case I is entirely stable. The figure shows that the instability persists for all intermediate w_0 solutions as $k \to 0$. The figure illustrates the tendency

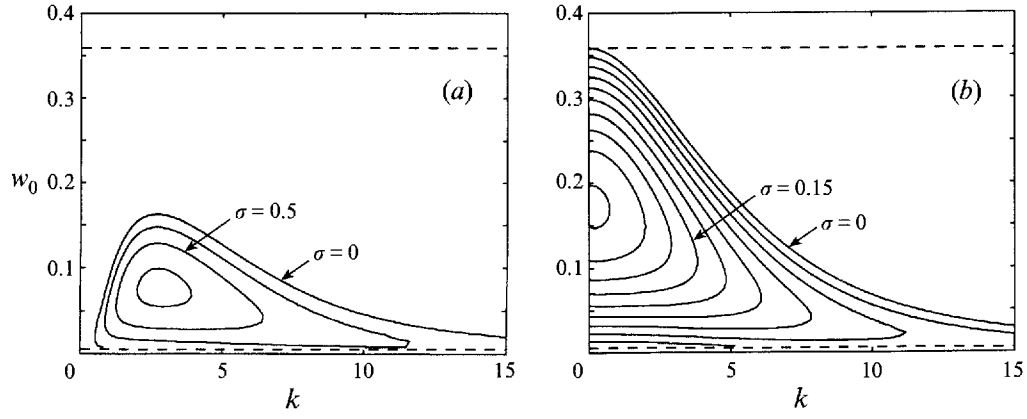

FIGURE 6. Same as figure 5, except $\gamma = 6$. (*a*) Case I. (*b*) Case II.

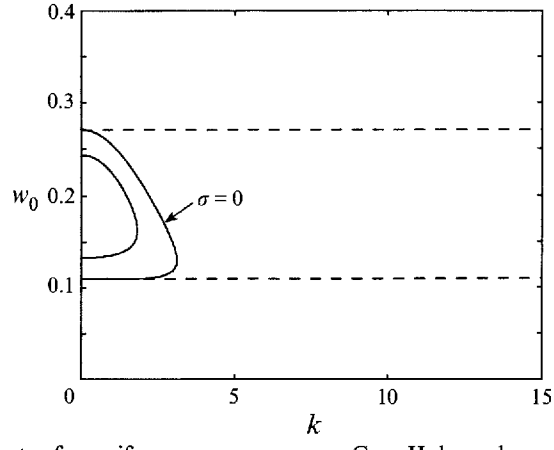

FIGURE 7. Growth rates for uniform source pressure, Case II, boundary conditions for $\gamma = 3.25$ and $\alpha = 0$. This example lies just into the multiple solution regime. At this value of γ the flow with uniform source flux boundary condition is entirely stable.

for high wavenumbers to stabilize as γ decreases and for the slow solution branch to stabilize.

With the constant-pressure boundary condition the instability is found for all $\gamma > \gamma_c$. In the uniform source flux case, the flow is unstable for only for $\gamma > 4.27$ (when $\alpha = 0$).

The effect of varying the buoyancy parameter α has not been studied thoroughly, but when $\alpha \leqslant O(1)$ computations show that it is destabilizing (stabilizing) for $\alpha > 0$ (< 0). This is also consistent with the effect of α on the basic-state flow solutions and is expected since for $\alpha > 0$ the fluid experiences a buoyancy force which acts to enhance the flow in the hot zones and retard the cold zones, thus reinforcing the basic instability. For $\alpha < 0$ the effect is opposite.

Typical unstable linear eigenfunctions, and their effect on the total flow, are illustrated in figures 8 and 9. Both figures are for an example with $\delta = 0.075$, $\gamma = 6$, $\alpha = 0$, and $k = \pi$ for the unstable intermediate solution $w_0 = 0.0829$. In figure 8 the uniform-flux (Case I) boundary condition (20) is used and in figure 9 the uniform-pressure (Case II) boundary condition (21) is used. In both figures the amplitude of the maximum temperature perturbation is set to 0.1 for the plots of

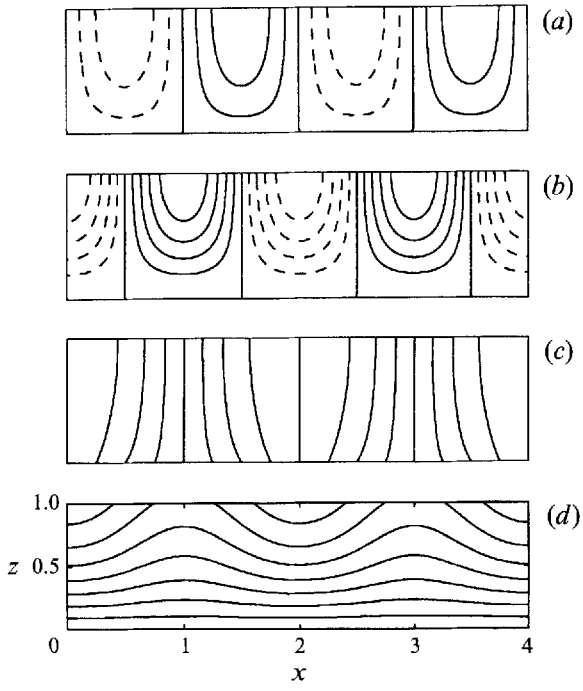

FIGURE 8. The unstable linear eigenfunctions for Case I and $\gamma = 6$, $\alpha = 0$, $\delta = 0.075$ ($w_0 = 0.0829$) and $k = \pi$. In (*a*) and (*b*) the pertubation streamfunction ϕ and temperature θ' are shown, respectively. The amplitude of θ' is set to 1. In (*c*) and (*d*) the total streamfunction ψ and temperature θ fields are shown for a maximum temperature perturbation amplitude of 0.1. The ψ-field is contoured in intervals of 0.05 and θ in intervals of 0.1.

the total fields (ψ, θ) (frames *c* and *d*). The perturbation fields (ϕ, θ') are shown in frames (*a*) and (*b*). The total temperature fields in the two cases are similar, with hot fluid localized into the fast-flowing zones which are separated by slow, cold viscous regions. The ψ-field (frame *c*) in Case II shows much less lateral flow. This feature helps to explain the stabilization at small k found for Case I (cf. figure 5*a*). With uniform flux at $z = 0$ all lateral flow must take place within the slot where the fluid is subject to cooling. As the wavelength of the instability increases some fluid parcels must follow a lengthening path from source to exit and therefore experience more cooling and an increasing viscosity.

5. Nonlinear evolution

The finite-amplitude evolution of the instability was explored by numerical integration of equations (17*a*,*b*) with the boundary conditions (18), (19) and (20), or (21). The temperature equation (17*b*) was integrated using second-order finite-differences in both space and time. The domain was taken to be periodic in the x-direction. The streamfunction ϕ was updated each time step by solving (17*a*) with θ' at the updated time. Equation (17*a*) was solved using a iterative under-relaxation method. The solution technique decomposed ϕ using a Fourier series in x and either finite differences in z for Case I, or a Fourier cosine series in z for Case II. A typical calculation had a resolution of 256 points in x and 40 points in z.

The initial conditions used were either the linear eigenmode solution (22) for runs

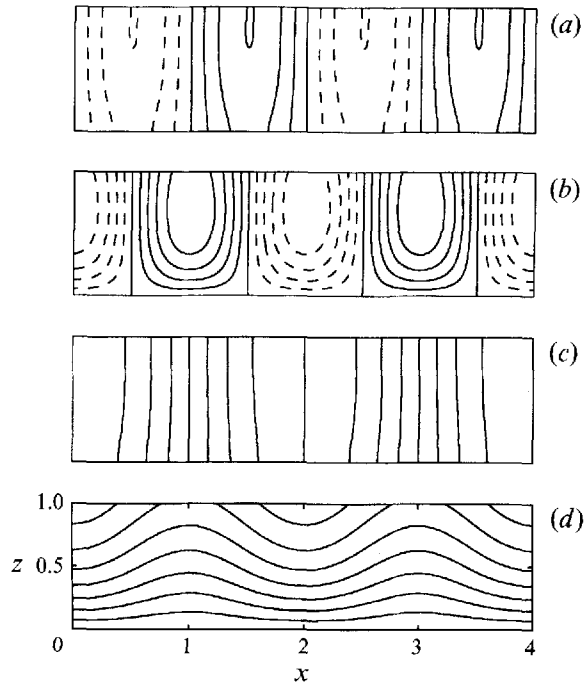

FIGURE 9. The same as figure 8, except with uniform source pressure, Case II, boundary conditions.

with disturbances of one wavenumber or, for initial disturbances composed of a spectrum of wavenumbers, $\phi = 0$ and

$$\theta' = \tfrac{1}{2}(1 - \cos 2\pi z) \sum_{n=1}^{N} a_n \sin(k_n x + \beta_n) \ .$$

Here a_n, β_n and $k_n = n2\pi/L_x$ are the amplitude, phase and wavenumber of mode n, respectively. L_x is the length of the domain in the x-direction.

A run with the initial condition consisting of one wavenumber is shown in figure 10. This example is for the uniform source flux boundary condition (Case I) with $w_0 = 0.0425$, $\delta = 0.075$, $\gamma = 5$ and $\alpha = 0$. The disturbance wavenumber $k = 3$ and $\sigma = 0.0344$. A maximum initial θ' amplitude of 0.015 is used. Figure 10(a) shows the total streamfunction ψ and figure 10(b) shows the total temperature θ. Time increases from top to bottom. The flow quickly focuses into hot zones of rapid flow ($t = 80$) which continue to narrow and increase in temperature and velocity ($t = 160$ and 240). At the last time there is evidence of the first harmonic ($k = 6$) present with the solution. Continued integration results in little change until $t \approx 560$ when the entire solution breaks down, apparently due to numerical problems. This is discussed below.

A run with the same parameters, but for the constant pressure source boundary condition (Case II) is shown in figure 11. The results are similar to those above, with focusing into hot, fast zones separated by broader, slow viscous zones by $t = 80$. In this case the growth rate $\sigma = 0.076$ and so the evolution is more rapid than for Case I. There is almost no lateral flow within the slot in this case and the width of the hot outflow zones at $z = 1$ is greater than for Case I. The solution remains essentially unchanged until $t = 200$ when the subharmonic $k = 1$ begins to appear, probably introduced as noise in the initial condition. Integration much beyond this time is not possible due to numerical problems. If the domain length is made to equal one

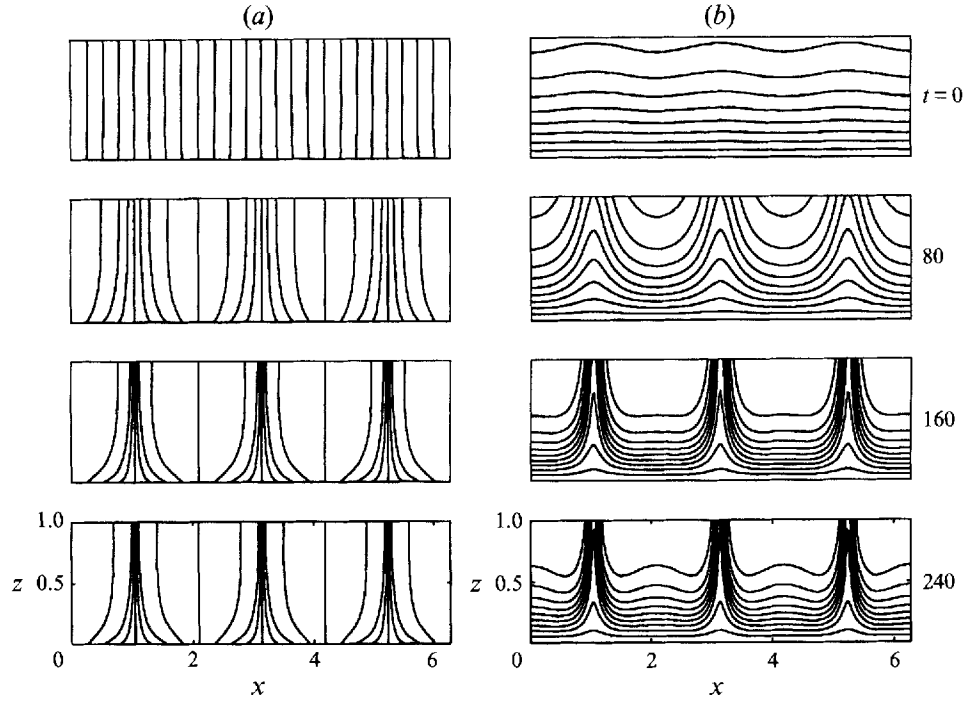

FIGURE 10. Nonlinear evolution for the uniform source flux, Case I, boundary condition with $\gamma = 5$, $\alpha = 0$, $w_0 = 0.0425$ ($\delta = 0.075$). The initial condition is the linear eigenmode for $k = 3$ ($\sigma = 0.0344$) with a maximum temperature perturbation amplitude of 0.015. Column (a) shows the total streamfunction ψ (contour interval of 0.0089) and (b) shows the total temperature θ (contour interval of 0.1).

disturbance wavelength $L_x = 2\pi/k$, the subharmonic is eliminated, but the numerical difficulties remain.

The evolution to a nearly steady finite-amplitude state is illustrated in figure 12, where the vertical velocity at two locations on the $z = 1$ boundary is shown as a function of time. One location is the centre of the hot zone at $x = \pi$ (solid line) and the other is in the cold zone at $x = 0$ (dashed line). The figure shows the results for the runs in figures 10 and 11. The Case I example (figure 10) is differentiated by the addition of circles. In both cases the flow reaches a nearly steady state after the initial growth period. This suggests that the finite-amplitude states are stable.

The inability to carry the integrations much further in time appears to stem from an inability to resolve the increasingly steep gradients. Convergence in the iterative solution for ϕ in (17a) cannot be achieved. Increasing the model resolution delays the onset of problems, suggesting a numerical origin of the difficulties. However, it may be that the strong viscosity and velocity gradients at the boundaries between the cold and hot zones are susceptible to a real instability of the type that occurs in viscosity stratified Couette flow (Craik 1969).

The numerical problems are reduced and the solutions approach true steady states as γ is reduced to just above the threshold for instability. As γ is increased the finite-amplitude solutions become increasingly more difficult to follow for long times. Again though, this is consistent with either a numerical resolution problem or a physical instability due to shear and viscosity gradients. Resolution of this issue is left for a later study.

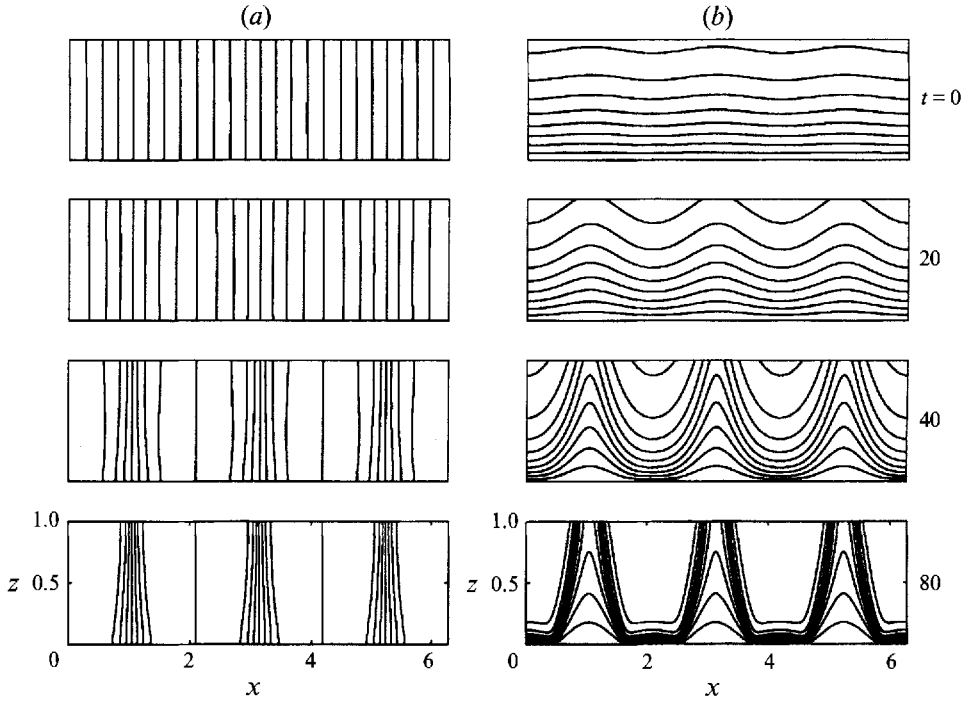

FIGURE 11. As figure 10 but for the uniform source pressure, Case II, boundary condition and $\sigma = 0.0763$.

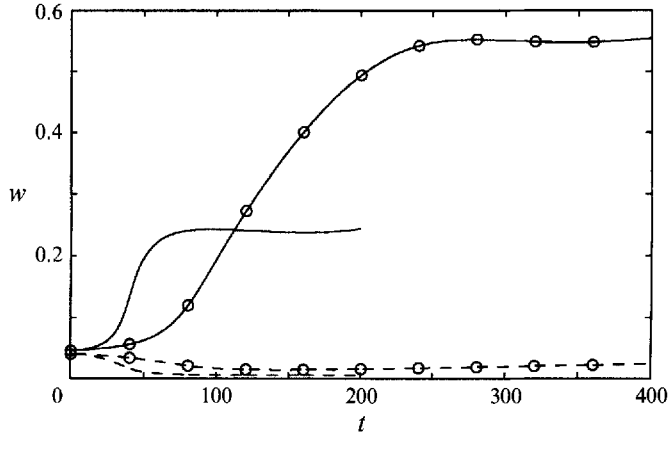

FIGURE 12. The vertical velocity at $z = 1$ at the centre of a hot zone ($x = \pi$) and a cold zone ($x = 0$) as a function of time for the runs in figures 10 and 11. The hot velocity is indicated by the solid line and the cold velocity by the dashed line. The results from figure 10, Case I, are marked by the circles.

Figure 12 shows that the finite-amplitude solutions evolve so that the vertical velocity in each zone (hot and cold) moves toward, but does not reach, the fast and slow branches of the basic-state flow solution. For the parameters of the runs in figures 10–12 the slow and fast solutions are $w_0 = 0.00921$ and 0.787, respectively. There is, however, no requirement that the flow achieve this state. The added lateral dimension is certainly important, and in Case I the pressure at $z = 0$ is not constant in x for $t > 0$.

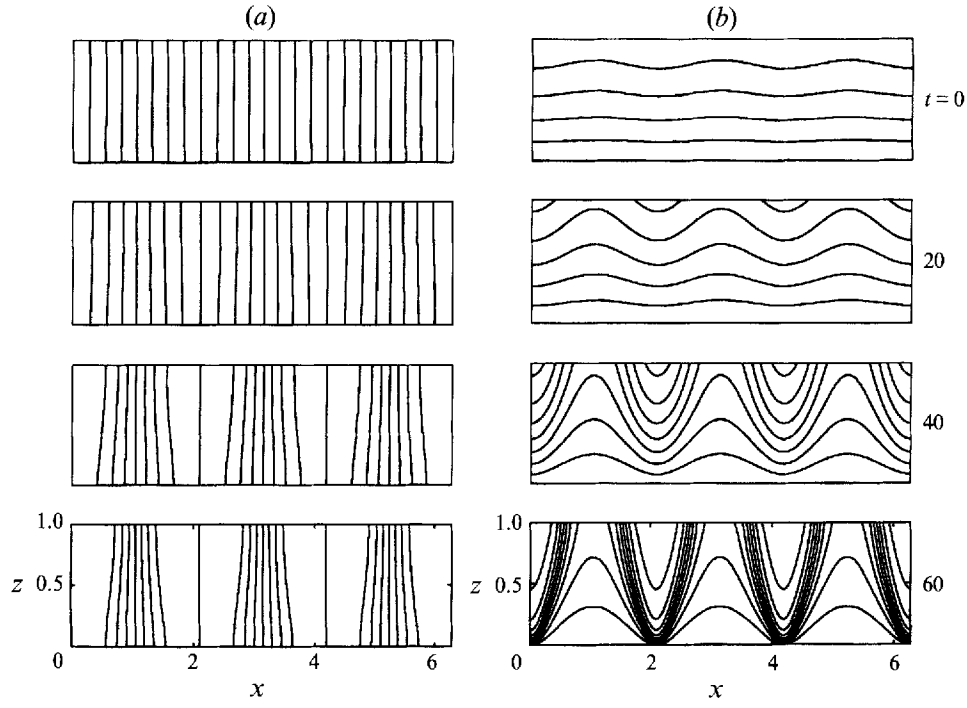

FIGURE 13. As figure 11 but with $w_0 = 0.2178$ ($\delta = 0.14$ and $\sigma = 0.0670$).

In these two runs the intermediate flow solution was relatively close to the slow branch solution. Or, recalling figure 2, the value of δ was close to the minimum for multiple solutions at the given γ. If δ is increased the solution remains qualitatively unchanged, but the width of the hot zones increases at the expense of the cold zones. This is illustrated in figure 13 where the evolution for the uniform source pressure boundary condition is shown for $w_0 = 0.2178$ ($\delta = 0.140$). The parameter settings $\gamma = 5$ and $\alpha = 0$ are unchanged from figure 11, to which this figure should be compared. This behaviour can be understood from continuity considerations. If over a wavelength the flow is assumed to adjust to a region of length l with velocity w_f, the fast solution to the basic state, and a region of length $1 - l$ with velocity w_s, the slow solution, then continuity gives $w_0 = (1 - l)w_s + lw_f$, or $l = (w_0 - w_s)/(w_f - w_s)$. Thus l increases (decreases) as w_0 approaches w_f (w_s).

These and other calculations demonstrate that for an initial disturbance of just one wavenumber the instability grows rapidly in place to a nearly steady final state. Changing the values of γ and α does not qualitatively affect the evolution.

Runs with an initial condition of a spectrum of wavenumbers are dominated at finite amplitude by low wavenumbers. This is illustrated for a Case II run with $\gamma = 5$, $\alpha = 0$, $\delta = 0.085$ and $w_0 = 0.0575$. The initial condition contained wavenumbers $k = 0.125$ to 7.5 in increments 0.125. All wavenumbers had equal amplitude and random phases. The linear stability analysis for the situation (see figure 5*b*) gives a fastest growing wavenumber at $k = 2.8$, though the growth-rate curve is nearly flat for $k \lesssim 4$. Shown in figure 14 are the ψ- and θ-fields at several times. At $t = 40$ several hot fingers are present, the strongest at $x = 22$. By $t = 50$ this finger dominates and carries most of the mass flux. Except for a weaker finger at $x \approx 29$, the rest of the fluid has slowed and is cooling, though there is still significant structure in the temperature field.

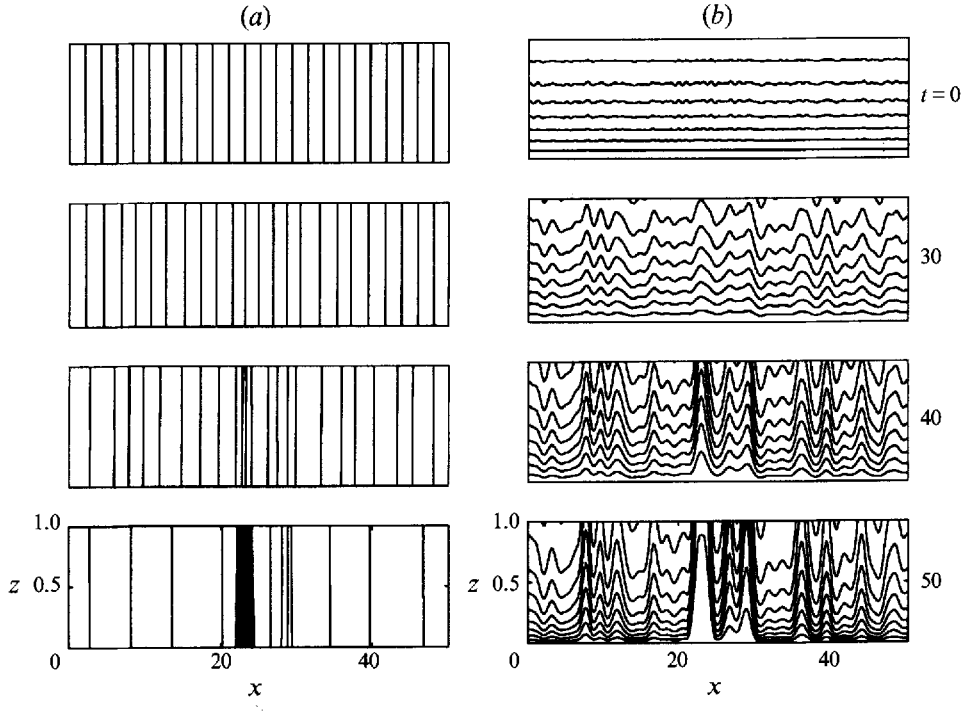

FIGURE 14. As figure 13 but the initial condition is a spectrum ($k = 0.125$ to 7.5 in increments of 0.125). Each wavenumber had the same θ' amplitude of 0.001 with random phase.

In figure 15 the Fourier amplitudes calculated from ϕ and θ' at $z = 1$ are shown for the same times as in figure 14. From the earliest time the ϕ-field is dominated by wavenumbers $k < 0.5$. In contrast, the spectrum of the temperature field is much more uniform. With time, cooling in the slow zones can be expected to reduce the energetic content of the higher wavenumbers.

Solutions with other realizations of the initial conditions, parameter values or boundary condition (Case I) exhibit the same behaviour. Dominance of low wavenumbers is a robust result of the nonlinear calculations.

6. Discussion

The work of WH on the instabilities of flows with temperature-dependent viscosity has been extended to permit lateral flow within the slot. This study also improves on their work by neglecting the inertial terms in the momentum equations and retaining time-dependence in the temperature advection equation. Both of these features are appropriate for the viscously dominated flows in question. The basic one-dimensional flow is subject to an instability in which relatively warm, low-viscosity, fluid is focused into fast-flowing channels separated by relatively slow, cold, and highly viscous zones. The temperature-dependence of the viscosity causes a feedback which enables the hot zones to flow even faster while the cold zones continue to slow, cool and increase in viscosity. The result is a thermo-viscous fingering instability. The necessary condition for instability is the presence of multiple (three) solutions for the basic-state vertical velocity. For the exponential viscosity-dependence studied here, multiple solutions occur for cold to hot viscosity ratios greater than 20.7.

The nonlinear calculations show that at finite amplitude the instability grows

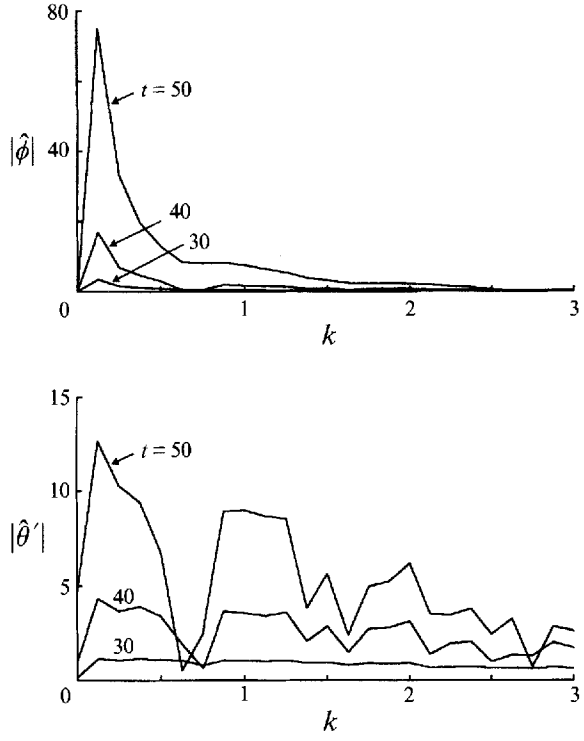

FIGURE 15. Amplitudes of the Fourier modes from the run in figure 14. (*a*) Fourier amplitudes of ϕ at $z = 1$. (*b*) Fourier amplitudes of θ' at $z = 1$. The times are indicated.

in place. The large-amplitude fingering state reaches a quasi-steady state that is apparently stable. For initial conditions consisting of numerous wavenumbers in the unstable band the calculations show that low wavenumbers are preferred at finite amplitude. The flow evolves to just a few widely spaced hot fingers, in qualitative agreement with the experiment of WH. Though more experimental work is necessary for a complete comparison and test of the model. This suggests that if the gap is of finite, rather than periodic, lateral extent the flow will evolve towards a final state with perhaps just one hot finger.

The relevance of these results to the stability of magma flow in dikes and fissure eruptions depends on the estimation of the parameters γ and δ. In dimensional variables these parameters are (see (11))

$$\delta = \frac{12\pi^2 \kappa \mu_H L^2}{P d^4}$$

and

$$\gamma = \gamma' (T_H - T_W) .$$

The wall temperature T_W is identified with the solidus temperature T_S of the magma. This is justified on thermodynamic grounds. Surrounding wall rock temperatures are likely to be even less than T_S.

The first condition for instability is that $\gamma > 3.03$ so that multiple solutions for the basic flow exist. This is easily met for basaltic magmas in the neighbourhood of their solidus temperature. From Shaw (1969) cold to hot viscosity ratios of $O(10^2$–$10^3)$ are typical for $T_H - T_W \gtrsim 100°\text{C}$, giving $\gamma \gtrsim 5$. This is well into the

multiple solution regime and the linear instability is possible if Case II, uniform source pressure, boundary conditions are used. This is the more realistic choice in the geological setting where we imagine that the slot is fed by a large magma source. While there must exist pressure variations within the chamber to facilitate lateral flow in the chamber, these are likely to be much less than the pressure drop from the slot entrance to the exit, due to the presumed larger size of the feeding chamber. So as a first approximation the source pressure can be considered uniform.

The second condition for instability is that the value of the heat transfer parameter δ lie in the region for multiple solutions for the basic state, or be larger so the solution lies on the slow branch. For $\gamma = 5$, figure 2(*b*) shows that $\delta \approx 0.056$–0.15 for multiple solutions. For typical values (Bruce & Huppert 1990, 1991) of slot length $L = 10^3$ m, $P/L = 2 \times 10^3$ Pa m^{-1}, $\kappa = 10^{-6}$ m^2 s^{-1} and $\mu_H = 10^2$ Pas, $\delta = 0.1$ for $d = 0.5$ m. While this estimate is within the unstable regime, it is meant only to illustrate that the instability is possible for reasonable geophysical parameters. The estimate for δ is very sensitive to the choice of d. Moreover, some of the other parameter estimates are not well constrained and may vary widely. A rough estimate for α, the buoyancy parameter, gives $\alpha \approx 0.1$, which is not large, but does enhance the instability.

It is important to re-emphasize that the model assumes cross-slot averages for all variables. This can lead to important quantitative differences when compared to models which do not average across the slot (Bercovici 1994; Wylie & Lister 1995). Recall from §2 that a consequence of cross-gap averaging was that γ in the averaged model is less than the γ of the real fluid. This suggests that the critical value of γ_c for the real fluid is larger than 3.03. Indeed, Wylie & Lister find a critical value of cold to hot viscosity ratio of $O(10^2)$, or $\gamma_c \approx 5$. This value is still such that the instability is possible for reasonable geophysical parameters. Even given these concerns, the present model improves on the earlier analysis of WH and helps to explain their experimental observations of thermo-viscous fingering.

While many details of the real geophysical problem, such as the role of the cross-gap dimension, a more precise consideration of the heat transfer to the surrounding wall rock and its insulating effect, the possibility of melting and freezing, and the coupled dynamics of the underlying magma chamber, have not been considered here, the present model illustrates the role of temperature-dependent viscosity on the focusing of magma flow in dikes and fissure eruptions. It offers a mechanism by which the flow internally focuses into narrow hot spouts, rather than focusing that depends on the initial gap structure as proposed by Bruce & Huppert (1989, 1990) in their model of the melt-back and freezing of dike walls. However, it should be noted that the mechanism of Bruce & Huppert can be qualitatively related to the present model. If instead of allowing the fluid viscosity to change, the gap thickness d is was permitted to change due to local melt-back or freezing, then much the same dynamics would probably occur. This can be seen by examining the momentum equations (1). A decrease (increase) in d is equivalent to an increase (decrease) in viscosity so far as it affects the flow resistance. This analogy between gap thickness and viscosity was also discussed by Stasiuk, Jaupart & Sparks (1993). The same feedback mechanism responsible for the thermo-viscous fingering would then result if faster flow produced melting (d increasing) and slower flow freezing (decreasing d), which does occur in the models of Fujii & Uyeda (1974), Turcotte (1990) and Bruce & Huppert (1989, 1990). It remains to be determined if multiple solutions for the basic flow exist. If yes, then an instability would be likely.

This work was funded by a grant from the National Science Foundation (EAR 87-08033). The author thanks J. Wylie and J. Lister for a preprint of their study and helpful comments on an early draft of this paper. J. Whitehead also contributed helpful comments on the work. Woods Hole Oceanographic Institution Contribution No. 8924.

REFERENCES

BERCOVICI, D. 1994 A theoretical model of cooling viscous gravity currents with temperature-dependent viscosity. *Geophys. Res. Lett.* **21**, 1177–1180.

BRUCE, P. M. & HUPPERT, H. E. 1989 Thermal control of basaltic fissure eruptions. *Nature* **342**, 665–667.

BRUCE, P. M. & HUPPERT, H. E. 1990 Solidification and melting along dikes by the laminar flow of basaltic magma. In *Magma Transport and Storage* (ed. M. P. Ryan) Wiley.

CRAIK, A. D. D. 1969 The stability of plane Couette flow with viscosity stratification. *J. Fluid Mech.* **36**, 685–693.

DELANEY, P. T. & POLLARD, D. D. 1982 Solidification of basaltic magma during flow in a dike. *Am. J. Sci.* **282**, 856–885.

FINK, J. H. & GRIFFITHS, R. W. 1990 Radial spreading of viscous-gravity currents with solidifying crust. *J. Fluid Mech.* **221**, 485–509.

FUJII, N. & UYEDA, S. 1974 Thermal instabilities during flow of magma in volcanic conduits. *J. Geophys. Res.* **79**, 3367–3369.

LISTER, J. R. 1994a The solidification of buoyancy-driven flow in a flexible-walled channel. Part 1. Constant volume release. *J. Fluid Mech.* **272**, 21–44.

LISTER, J. R. 1994b The solidification of buoyancy-driven flow in a flexible-walled channel. Part 2. Continual release. *J. Fluid Mech.* **272**, 45–65.

LISTER, J. R. & KERR, R. C. 1991 Fluid-mechanical models if crack propagation and their application to magma transport in dykes. *J. Geophys. Res.* **96**(B6), 10049–10077.

OCKENDON, H. & OCKENDON, J. R. 1977 variable viscosity flows in heated and cooled channels. *J. Fluid Mech.* **83**, 177–190.

RICHTER, D. H., EATON, J. P., MURATA, K. J., AULT, W. U. & KRIVOY, H. L. 1970 Chronological narrative of the 1959–60 eruption of Kilauea Volcano, Hawaii. *US Geol. Surv. Prof. Pap.* **537-E**, 1–73.

RYAN, M. P. & BLEVINS, J. Y. K. 1987 The viscosity of synthetic and natural silicate melts and glasses at high temperatures and 1 bar (10^5 pascals) pressure and at higher pressures. *US Geol. Surv. Bull.* **1764**, 563.

SHAW, H. R. 1969 The rheology of basalt in the melting range. *J. Petrol.* **10**, 510–535.

STASIUK, M. V., JAUPART, C. & SPARKS, R. S. J. 1993 On the variations of flow rate in non-explosive lava eruptions. *Earth Planet. Sci. Lett.* **114**, 505–516.

TURCOTTE, D. L. 1990 On the role of laminar and turbulent flow in buoyancy driven magma fractures. In *Magma Transport and Storage* (ed. M. P. Ryan) Wiley.

WHITEHEAD, J. A. & HELFRICH, K. R. 1991 Instability of flow with temperature-dependent viscosity: A model of magma dynamics. *J. Geophys. Res.* **96**(B3), 4145–4155 (referred to herein as WH).

WYLIE, J. J. & LISTER, J. R. 1995 The effects of temperature-dependent viscosity on flow in a cooled channel with application to basaltic fissure eruptions. *J. Fluid Mech.* **305**, 239–261.